Synthesis and superconducting properties of a Rb_3C_{60} single crystal

Shaoyan Chu and Michael E. McHenry
Department of Materials Science and Engineering, Carnegie-Mellon University, Pittsburgh, Pennsylvania 15213
(Received 31 January 1996; revised manuscript received 21 January 1997)

A pristine Rb_3C_{60} single crystal with larger than millimeter dimensions was prepared by reaction of rubidium vapor with a seed-grown C_{60} single crystal (which exhibited remarkably sharp x-ray-diffraction peaks). A narrow superconducting transition width ΔT_c (5–85 % diamagnetic shielding) of the Rb_3C_{60} single crystal is less than 1 K. The onset of the transition was at a temperature, $T_c = 30.0$ K. Measurements of temperature dependence of the zero-field-cooled and field-cooled dc magnetization (using ten applied magnetic fields up to 5.0 T) are reported here. These and magnetization vs field data at different temperatures (ranging from 2 to 29 K) have been used to determine thermodynamic superconducting parameters, including the lower $[H_{c1}(T)]$ and upper $[H_{c2}(T)]$ critical fields, the Ginsburg-Landau coherence length ξ, and the London or Ginzburg-Landau penetration depth, λ. These are significantly different from those extracted from similar data in the literature for powder specimens. Hysteresis and magnetic relaxation measurements have been used to determine the nominal critical current density $J_c(H,T)$ and the effective-pinning potential $U_{\text{eff}}(J,H)$, respectively. [S0163-1829(97)10717-2]

I. INTRODUCTION

The discovery[1–3] of a new family of superconductors, alkali-doped C_{60} compounds, has stimulated substantial theoretical and experimental interest. The basic properties of a superconductor, such as the thermodynamic critical field H_c, the Ginsburg-Landau (GL) parameter κ, the magnetic-field (London) penetration depth λ, and the Ginsburg-Landau coherence length ξ, provide insight into the superconducting mechanism as well as useful information for understanding the flux-pinning mechanism. The difficulties in correctly determining these fundamental quantities in alkali-doped C_{60} superconductors have been recognized as resulting from their variable composition, instability with respect to oxidation, and the problems associated with growing large single crystals.

Investigations of M_xC_{60} (M is Na, K, Rb, Cs, and their binary mixture) in the range $1<x<6$ have been reported.[4] Among the alkali-doped C_{60} compounds, the line compound M_3C_{60} is the only superconducting phase. Experimental results reported in the literature have given widely varying estimates for the values of the London penetration depth λ and Ginsburg-Landau coherence length ξ. These estimates have been based on magnetization measurements of K_3C_{60} (Ref. 5) and Rb_3C_{60} (Ref. 6), powder or resistance measurements on thin films[7] and crystals[8] of K_3C_{60}. Obtaining reliable values has proved to be an experimental challenge. For lack of large single crystals the pinning of M_xC_{60} materials and the anisotropy effects in the cubic superconductors have also been largely unexplored. This has motivated us to prepare and to characterize a series of large single crystals of alkali-doped C_{60}. Not only do these experimental efforts attempt to provide measurements of fundamental superconducting properties in high-quality single crystals, but also to illuminate differences in behavior between isotropic and anisotropic high-temperature superconductors. With a transition temperature of 30 K and a cubic structure, Rb_3C_{60} is an excellent example of an isotropic high-temperature superconductor. Many aspects of superconducting fluctuations, anomalous H-T phase diagrams, and weak pinning in high-temperature superconductors have been attributed to anisotropy and reduced dimensionality. It is therefore desirable to compare high-temperature superconductors (HTSC's) with notable anisotropy with *cubic* HTSC materials.

While determination of equilibrium thermodynamic critical fields and length scales are always important in describing the superconducting state, nonequilibrium properties associated with flux pinning in type-II superconductors are also quite important in determining their potential in high-field and high current applications. Here we also report hysteretically determined critical current densities, $J_c(H,T)$, for large Rb_3C_{60} single crystals using a Bean model analysis for a superconducting slab.[9] Further magnetic relaxation data has been taken as an attempt to determine the nonlinear effective flux-pinning potential for these materials.[9–11]

II. EXPERIMENTAL PROCEDURE

The high-quality C_{60} crystal used in this study was cut from a bar-shaped single crystal that was grown from a seed crystal using a gas-phase (sublimation) growth procedure. Raw C_{60} powder (MER corporation, 99.5%) was refined by sublimation in a vacuum quartz tube. In the vapor-phase crystal growth ~100 mg of C_{60} extract was heated to ~560 °C in an evacuated quartz ampule where it sublimed. The C_{60} vapor phase follows the natural temperature gradient in the furnace to the cold end of the tube where we had made a few scratches on the inside wall. Here C_{60} recondenses to form many nuclei of the crystalline solid which grow as a function of time. After we observed the crystallites to nucleate on scratches in the quartz ampule, we tilted and vibrated the cold end of the ampule to cause the nuclei to fall down so that only a few of them remained as crystal seeds. We have demonstrated larger bar-shaped crystals can be grown from these seeds.

The structure and dimensions of the raw C_{60} crystal were

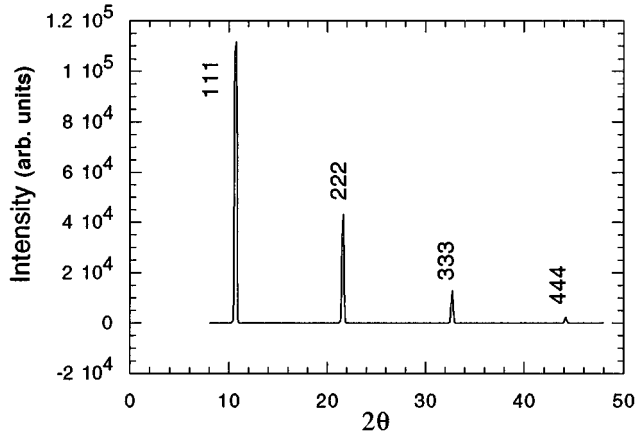

FIG. 1. X-ray-diffraction pattern for a pure C_{60} crystal taken using Cu K_α radiation incident on a [111] surface.

checked by x-ray-diffraction (XRD) pattern and optical microscopy. The well-known fcc crystal structure of the pure C_{60} crystal with a lattice parameter of $\sim$14.18 Å has been observed. From the systematics of the variation of x-ray-scattered intensity with orientation, we were also able to determine that the [111] direction of the lattice is perpendicular to the largest surface of the crystal. With the exception of a cut face, each of the surfaces of the crystal was a regular plane with metallic luster, indicating that these faces were free surface when this crystal grew. Using crystal mass, $m = 1.03$ mg, and microscopically determined crystal dimensions we found the crystal's density to be $\rho = 1.65$ g cm^{-3}. This value is in close agreement with the 1.67 g cm^{-3} density determined based on the XRD determined fcc lattice parameter. The diffraction pattern for the pure C_{60} crystal, before doping Rb, is shown in Fig. 1.

The variety of experimental procedures which have been used to prepare alkali-doped C_{60} superconductors can be construed as influencing the variation of properties observed in the literature. In particular, in the measurement of fundamental thermodynamic superconducting properties it is highly desirable to make measurements on a single crystal with the orientation of magnetic field with respect to the crystal axes well known. The sample used in the present work was prepared from a solid-gas reaction of pristine C_{60} single crystals reacted with rubidium vapor. A wide compositional range was explored (molar ratios, Rb:C_{60}, from 1 to 8) and different heat treatments were used so as to maximize the superconducting shielding fraction of the resulting doped crystals.

Our standard synthesis procedure consisted of sealing several millimeter-sized pure C_{60} crystals and a piece of rubidium (Rb, Alfa, 99.95%) in a vacuum Pyrex tube. The C_{60} crystals were placed in the hot end of a horizontal furnace at $\sim$200 °C (well below the C_{60} sublimation temperature). The rubidium source end was held at an optimum temperature which ranged from 190 to 195 °C. A higher temperature helps in completing the $x\mathrm{Rb}+\mathrm{C}_{60}=\mathrm{Rb}_x\mathrm{C}_{60}$ reaction. However, too high a reaction temperature may lead to cracking and evaporation of the crystal grain. A slight excess of rubidium (compared to the minimum necessary for a Rb_3C_{60} stoichiometry) was observed to increase superconducting shielding diamagnetic fraction of the product. Depending on the C_{60} crystal size and the reaction temperature, the heat treatment time varied from one day to ten days. The quality of the superconducting Rb_3C_{60} single crystals correlated with keeping their original shape, even though crystal surfaces lost their metallic luster and became opaque.

Part of the resulting crystal was cut from the doped crystal used in this work for x-ray-diffraction analysis. The volume of the remnant Rb_3C_{60} single crystal for magnetic measurements was approximately 0.57×10^{-3} cm^3. The Rb_3C_{60} single crystal was frozen in a pellet of polyethylene to prevent moisture or air from damaging the superconducting phase. This also had an advantage over sealing in a Pyrex tube which usually contributes a larger (temperature independent) diamagnetic background signal. It was confirmed that the magnitude of the sample magnetization remained constant for at least ten weeks indicating that the polyethylene seal impeded oxidation of Rb in the single-crystal sample. The sample was stored in an evacuated sealed quartz ampule and transferred in air between measurements.

A superconducting quantum interference device (SQUID) magnetometer (Quantum Design, San Diego, California) was used to measure the dc magnetization of the sample in field up to 5 T in temperature down to 2 K. Using the MPMS2 model with a scan length of 3 cm, yields a field variation of less than 0.05% over the scan length. The system temperature was always within ±0.02 K of the target temperature prior to measurement. For investigating possible anisotropic properties of the doped fullerenes, we arranged the magnetization measurements to be carried out with applied magnetic field parallel to the [111] direction and [112] direction of the crystal lattice, respectively. We use left subscripts 1 and 2 to indicate the two different orientations. In this work, only the data measured with the field oriented in the [111] direction are analyzed in detail. As a comparison several experimental results with the field oriented in the [112] direction are also discussed in this work. In a subsequent work we will compare length scales (coherence lengths and penetration depths) for the [111] and [112] directions using a formalism of crystalline anisotropy and Fermi-surface anisotropy for fullerene superconductors with a cubic lattice structure.

III. RESULTS AND DISCUSSION

At the outset we alert the reader that we present an initial analysis of our first magnetization results using standard analytical techniques to determine critical fields, thermodynamic length scales and nonlinear effective-pinning potentials. We attempt to estimate these quantities and compare our results to what we believe to be less accurate powder results and results for small single crystals. We will discuss orientational effects (field orientation with respect to crystallographic axes) in a future publication. Here we explore in Sec. III A, the superconducting transition temperature for our crystal, in Sec. III B, the zero-field-cooled (ZFC) and field-cooled (FC) susceptibilities and the Meissner effect, in Sec. III C, the lower H_{c1}, upper H_{c2}, and thermodynamic critical fields H_c and length scales, and in Sec. III D, hysteretic response and pinning potentials.

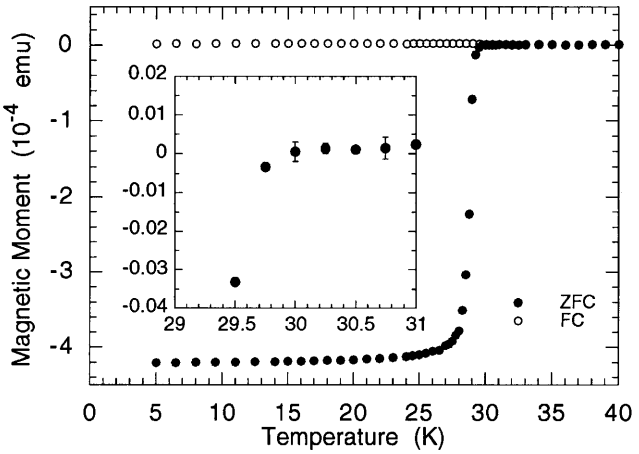

FIG. 2. Temperature dependence of the zero-field-cooled (ZFC) and field-cooled (FC) dc magnetic moment with a fixed applied field of 2 Oe. The volume of the single crystal is 0.57 $\times 10^{-3}$ cm^3.

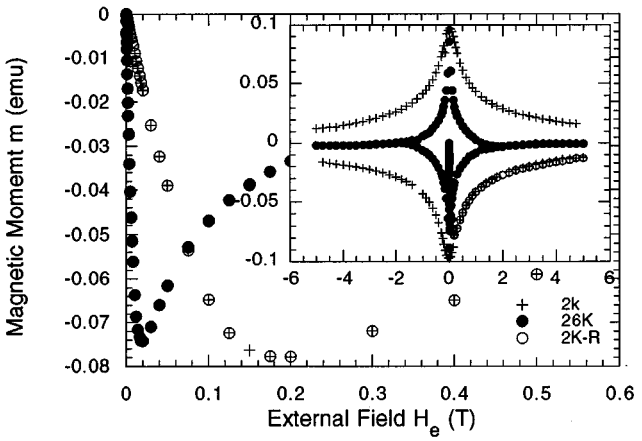

FIG. 3. Magnetic-field dependence of the magnetization at a fixed temperature $T=2$ and 26 K. After three weeks' interval, the superconducting diamagnetic signal (open circles) shows the same value as before (crosses).

A. Superconducting transition temperature

The superconducting transition temperature was determined from measurements of the temperature dependence of the zero-field-cooled (ZFC) and field-cooled (FC) temperature dc magnetic dipole moment (emu) of the Rb_3C_{60} single crystal as illustrated in Fig. 2. The following experimental protocol employed: (a) the sample was first cooled from its normal state (above 40 K) to 5 K in zero field ($<$0.5 Oe); (b) its dc magnetic moment was monitored as a function of increasing temperature as the sample was heated above superconducting transition temperature T_c in an applied field of 2 Oe (ZFC); and (c) it was subsequently cooled to 5 K under the same field (FC).

Using a linear extrapolation above the onset of the superconducting diamagnetic transition, T_c was determined to be 30.0 K. The full width of the transition 5–85 % is less than 1 K. The sharpness of the transition is consistent with the high quality of our sample. The thermomagnetic hysteresis between the FC and ZFC susceptibilities is consistent with flux being trapped in the sample as it is cooled below the transition temperature. It should be mentioned that from a ZFC susceptibility measurement in an applied field of a few Oe one can only roughly estimate a diamagnetic shielding fraction, because uncertainty of remnant field trapped in the SQUID system's superconducting solenoid as well as contributions from the earth's field.

B. FC and ZFC susceptibility, Meissner effect

Perfect diamagnetic shielding would be reflected in an experimental susceptibility χ_e given by

$$x_e=\frac{M}{H_e}=\frac{M}{H_i+4\pi DM}=-\frac{1}{4\pi(1-D)}. \qquad (1)$$

Here M is magnetization, D is the demagnetization factor, and H_e and H_i are the external (applied) magnetic field and internal magnetic field, respectively. The demagnetization factor can be estimated for our sample using the formula for an oblate spheroid with an identical aspect ratio. For a more precise determination, however, we made a lead replica of the Rb_3C_{60} single crystal and measured its demagnetization factor experimentally. The magnetic-field dependence of dc magnetization of the lead replica yielded a demagnetization factor, ${}_1D$, for this geometry, of 0.57, in the case of an applied field parallel to the shortest dimension of the replica.

The magnetic-field dependence of the dc magnetization of the Rb_3C_{60} single crystal from zero field ($<$0.5 Oe) to a maximum applied field of 5 T and for fixed temperatures between $T=2$ and 26 K is shown in Fig. 3. The data were taken with the same field orientation as used in determining ${}_1D$ with the lead replica (i.e., in the [111] direction for the fcc crystal lattice). The shielding magnetization remains linear in an applied field until flux lines start to enter the crystal at the lower critical field H_{c1}. Using the low-field data (in the linear regime) the calculated shielding fraction of our sample is about 80% of that predicted for a perfect diamagnet using Eq. (1). Here we neglect reduction of the susceptibility due to edge effects. These results were reproducible after a three week interval indicating little deleterious degradation of properties due to oxidation of Rb over this time.

C. Critical fields and thermodynamic length scales

For determining upper critical field H_{c2}, we show the temperature dependence of the ZFC and FC dc magnetization at various fixed applied fields in Fig. 4. The data were gathered using the same protocol as for the low-field (2 Oe) data described above. Compared with the superconductor's diamagnetic signal, the contribution from the sample rod, the polyethylene pellet, and a straw sample holder (also polyethylene), was small. Nonetheless, in order to insure accurate fits to $M(T)$ for the single crystal, a correct subtraction of the background signal is extremely important, especially at high field. Magnetization versus temperature was measured at various fixed magnetic-fields from superconducting transition temperature to 40 K. We fit the background magnetization at fixed applied field using a form: $(AT^{-1}+B+CT)$ which included diamagnetic term due to the polyethylene (nearly T independent) and paramagnetic term attributed to the Rb_3C_{60} normal. This form was extrapolated to low tem-

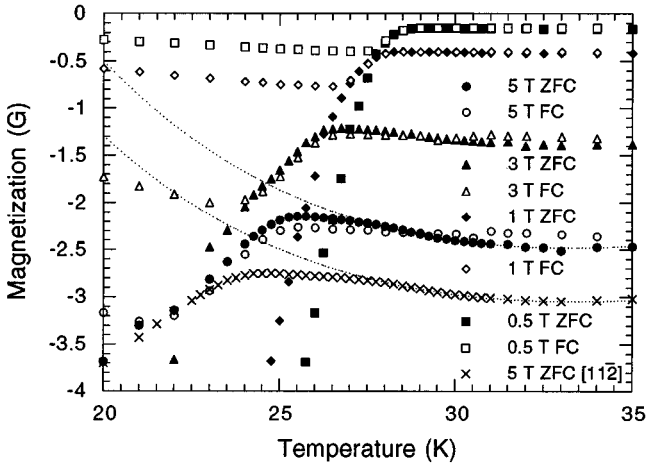

FIG. 4. Magnetization vs temperature measured near ${}_1T_c(H)$ in different field 0.5, 1, 3, and 5 T for ZFC and FC. Data in other applied fields were not shown for clarity. The arrow indicates the irreversible temperature $T_{\rm irr}$ of $\sim$22 K at $H=5.0$ T. A basal line (dashed) for the ZFC curve at the applied field 5 T was determined from the data obtained above the transition temperature (see text). As a comparison, the temperature dependence of magnetization of the sample with the field orientated in the [112] direction is also shown in this figure.

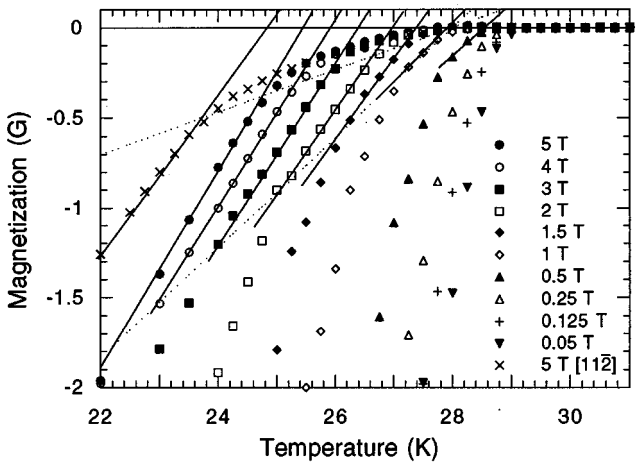

FIG. 5. Temperature dependence of the ZFC magnetization with the background signal subtracted. The solid lines are fits to Eq. (2) over a temperature range (indicated between two dashed lines) between $T_{\rm irr}$ and the temperature at which magnetic fluctuations are evident. A ZFC magnetization curve with [112] field orientation ($H=5$ T) has been shown in same figure.

peratures and subtracted from $M(T)$ to obtain the net, superconducting response of the Rb_3C_{60} single crystal in fixed fields from 0.05 to 5 T.

In temperatures between 20 and 35 K demagnetization corrections are neglected because of very small sample magnetization. The irreversibility temperature, $T_{\rm irr}$, is identified as the separation point between the ZFC and FC curves. Above $T_{\rm irr}$ and below T_c a linear temperature dependence of the magnetization is observed. In this range the superconducting order parameter and thus the magnetization is proportional to temperature.[12] In a critical region a broadening of the transition temperature $T_c(H)$ is caused by superconducting diamagnetic fluctuations and inhomogeneity of the sample, and the temperature dependence of magnetization is no longer linear. The magnetic fluctuation region may extend to $\sim$5 K below the zero-field transition, $T_c(0)$, at $H=5$ T.

The nucleation temperature, $T_c(H)$, is commonly defined as an intercept of a linear extrapolation of the $M(T)$ curve with the $M=0$ axis, which has been corrected for background signal as described above. This linear extrapolation has been shown to be inadequate for very anisotropic superconductors[13] as a result of quasi-two-dimensional diamagnetic fluctuations [in the extreme leading to a $T_c(H)$ determined by linear extrapolation which increases with field]. For the *cubic* crystal we observe a field and temperature regime for which the linear extrapolation adequately describes $T_c(H)$. Figure 5 shows a linear extrapolation of $M(T)$ in a temperature range beyond the fluctuation regime. We also note that, at lower field ($<$0.5 T) the values of $T_c(H)$ were evaluated only at a temperature where the Meissner effect is no longer observed in a ZFC measurement.

We emphasize that the upper critical field $H_{c2}(T)$ of the fullerene superconductor Rb_3C_{60} is dependent on the field orientation. As shown in Figs. 4 and 5, the nucleation temperature, ${}_1H_{c2}(5T)$, is obviously higher than ${}_2H_{c2}(5T)$. To our knowledge, the anisotropy of the upper critical field in fullerene superconductors has not yet been observed, even though strong effects of the anisotropy on the magnetic properties of conventional cubic superconductors are well known.

We plot ${}_1H_{c2}(T)$ vs H in the inset of Fig. 6. Above 1.5 T, a straight line corresponds to an upper critical field slope $\partial_1 H_{c2}(T)/\partial T=-1.95$ T/K and a GL transition temperature ${}_1T_{c\ \rm GL}(0)=28.0$ K. For applied fields less than 1.0 T, the values of $\partial_1 H_{c2}(T)/\partial T$ deviate from that of the linear fit and exhibits notable curvature as has been observed in many other publications.[5,8,14,15] In this range, the slope, $\partial M/\partial T$, of the fixed field magnetization decreases with decreasing values of $\partial_1 H_{c2}(T)/\partial T$ as is shown in Fig. 5. This is consistent with solutions to linearized Ginzburg-Landau equations for $M(T)$ near $H_{c2}(T)$ (Ref. 12).

$$4\pi M=-\frac{H_{c2}-H_e}{1.16(2\kappa^2-1)} \tag{2}$$

for a triangular Abrikosov vortex lattice structure. In this regime the value of Ginzburg-Landau parameter κ is taken as being independent of temperature.

Using Eq. (2) to determine $H_{c2}(T)$ can be problematic if the data are inadequate to reliably determine the partial derivative of the magnetization with respect to temperature, $\partial M/\partial T$. This will be the case when the irreversible regime and the fluctuation regime nearly coincide, compressing the linear $M(T)$ regime and compromising fits which rely on an accurate determination of $\partial M/\partial T$. Another method for determining $H_{c2}(T)$ relies on fits using the London intermediate-field regime expression: $4\pi M=\phi_0/8\pi\lambda_L{}^2\ln(\eta H_{c2}/H)$ (where η is a constant on the order of unity). Though this characteristic $\ln(H)$ dependence has often been observed in the intermediate-field regime, it has recently been pointed out that the London model is quantitatively incorrect because of its failure to address energetic contributions due to the cores. Recently, a variational

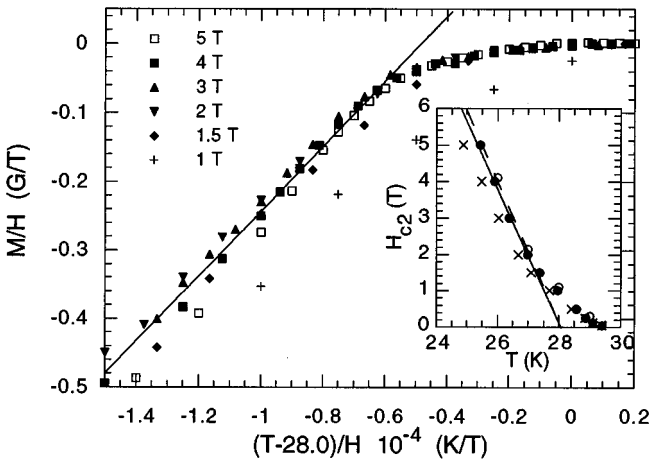

FIG. 6. A scaling of the magnetization data measured at 1.0, 1.5, 2.0, 3.0, 4.0, and 5.0 T by using Eq. (3). Inset: The temperature dependence of the upper critical field $H_{c2}(T)$. Solid dots are defined in Fig. 4. Open circles are from hysteresis curves $M(H)$ at $T=26$, 27, 28, and 29 K. The solid line is a fit to the solid dots at fields above 1.5 T. The dashed line is from the scaling relation, Eq. (3) with $-1.2<(T-T\mathrm{GL})/H<-0.6$ (K/T) and H_e between 1.5 and 5.0 T. Crosses are ${}_2H_{c2}(T)$ data.

model[16] which treats the cores explicitly has been shown to yield a more accurate description of the magnetization in the intermediate-field regime. This model also lends itself to fits of a $\ln(H)$ form for which $-4\pi M=\alpha\phi_0/8\pi\lambda_L{}^2\ln(\beta H_{c2}/H)$, where α and β are two fitting parameters to the variational model. Unfortunately this fitting procedure is also inconvenient for analysis of our data since the magnetization of fullerenes superconductors has a narrow reversible range and a large magnetic fluctuation. Any such an analysis based on $\partial M/\partial H$ or $\partial M/\partial T$ will be ambiguous unless there are enough data to accurately fit the slopes.

We suggest here a fitting procedure which uses plots of M/H vs $[T-T_{c\mathrm{GL}}(0)]/H$ (K/T) to determine $H_{c2}(T)$. This procedure relies on the equation

$$\frac{M}{H_e}=\frac{1}{4.64\pi(2\kappa^2-1)}\left[\left(-\frac{\partial H_{C2}(T)}{\partial T}\right)\times T_c\left(\frac{T-T_{C\mathrm{GL}}(0)}{H_e}\right)+1\right], \tag{3}$$

derived by differentiating Eq. (2) within the reversible transition regime. Here the Ginzburg-Landau transition temperature $T_{C\mathrm{GL}}(0)$ is usually several degrees smaller than $T_c(0)$. We have used Eq. (3) to fit our magnetization data taken at fixed field between 0.5 and 5.0 T, as illustrated in Fig. 6. In these fits $T_{C\mathrm{GL}}(0)$ is the only adjustable parameter. Excellent agreement between the theory and experiment is clearly illustrated for fields exceeding 1.5 T. It is expected that this scaling should prove inadequate at lower fields where nonlinearity in ${}_1H_{c2}(T)$ vs T is clearly evident.

Fits to Eq. (3) in the temperature regime between the irreversible temperature and the temperature where an obvious magnetic-fluctuation effect appears are also shown in Fig. 6. A fit of Eq. (3) in the regime $-1.2<(T-T_{\mathrm{GL}})/H<-0.6$ (K/T) yields ${}_1T_{c\mathrm{GL}}(0)=28.0$ K, $\partial_1 H_{c2}(T)/\partial T=-2.08$ T/K, and ${}_1\kappa=39.2$. These values are similar to those obtained by the simple linear fits to Eq. (2), however, the latter fitting procedure is more robust in avoiding ambiguities in determining $\partial M/\partial T$ and $\partial H_{c2}(T)/\partial T$. The consistency of this approach has been checked by evaluating the slope of magnetic hysteresis curves, $M(H)$, at fixed temperatures near $T_c(H)$. Using the equation

$$\frac{\partial M}{\partial H_e}=\frac{1}{4.64\pi(2\kappa^2-1)}, \tag{4}$$

arrived by differentiating Eq. (2) with respect to field, we obtain GL parameter ${}_1\kappa=39.8$, 38.7, 39.3, and 37.5, for $T=26$, 27, 28, and 29 K. The ${}_1H_{c2}(T)$ values derived from hysteresis data at these temperatures are shown in the inset of Fig. 6. All of the data are in very good agreement with the results of the fits of $M(T)$ curves in Fig. 5.

The zero-temperature GL coherence length, $\xi_{\mathrm{GL}}(0)$, is the value of $\xi_{\mathrm{GL}}(T)$ extrapolated to 0 K. The fact that the upper critical field $H_{c2\mathrm{GL}}(0)$ represents the field at which fluxon cores of radius $\xi_{\mathrm{GL}}(0)$ overlap allows us to relate $H_{c2\mathrm{GL}}(0)$ and $\xi_{\mathrm{GL}}(0)$:

$$H_{C\mathrm{GL}}(0)=\frac{\phi_0}{2\pi\xi_{\mathrm{GL}}^2(0)}. \tag{5}$$

To determine the 0-K value of H_{c2}, $H_{c2\mathrm{GL}}(0)$, we use Werthamer-Helfand-Hohbenberg[17] (WHH) formula:

$$H_{c\mathrm{GL}}(0)=-0.69\left[\frac{\partial H_{c2}(T)}{\partial T}\right]\Bigg|_{T_c}T_c, \tag{6}$$

which yields ${}_1H_{c2\mathrm{GL}}(0)=43.0$ T and ${}_1\xi_{\mathrm{GL}}(0)=27.7$ Å for our single crystal. These values are quite different from those obtained from magnetic measurements[6] on a powder sample, but similar to those obtained from ac susceptibility measurements.[18,19] Assuming $\kappa=\lambda/\xi$ to be independent of temperature we estimate the penetration depth ${}_1\lambda_{\mathrm{GL}}(0)=1090$ Å corresponding to ${}_1\kappa=39.2$ and ${}_1\xi_{\mathrm{GL}}(0)=27.7$ Å. This value is only about half of that observed by Sparn *et al.*,[6] but close to the 1200–1400 Å determined by Politis, Sokolov, and Buntar[15] and also close to a theoretical estimation based on band-structure calculations for K_3C_{60}.[17] Similar inconsistencies in values of the penetration depth have been noted by Palstra *et al.*,[7] Hou *et al.*,[8] and Foner *et al.*[20] for length scales determined by resistance measurements on the fullerene-based superconductor K_3C_{60}.

The large uncertainty in the values of the penetration depth reflects the experimental difficulty in determining the lower critical field, H_{c1}. Again in Ginzburg-Landau theory, H_{c1} can relate to the GL penetration depth, λ, and κ:

$$H_{c1}=\frac{\phi_0}{4\pi\lambda_{\mathrm{GL}}^2}\ln\kappa. \tag{7}$$

Noting the deviation from a linear $M(H)$, we estimate ${}_1H_{c1}(0)$ should be about 0.05 T. This value is in good agreement with the 0.045 T value of Politis, Sokolov, and Buntar[15] but much larger than the 0.012 T determined by Sparn *et al.*[6] Buntar, Eckern, and Politis[21] have discussed the experimental challenges in determining H_{c1} from magnetization curves. Despite these challenges we interpret a set of

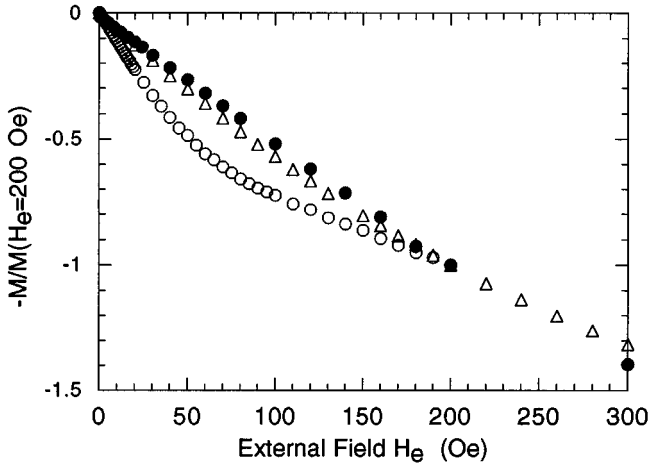

FIG. 7. Magnetic-field dependence of $-M/M(H_e=200\ \mathrm{Oe})$ at 5 K used for determining lower critical field ${}_1H_{c1}$. Open circles and triangles are from Sparn *et al.* (Ref. 6) and Politis, Sokolov, and Buntar (Ref. 15), respectively. Solid dots show the data in this work.

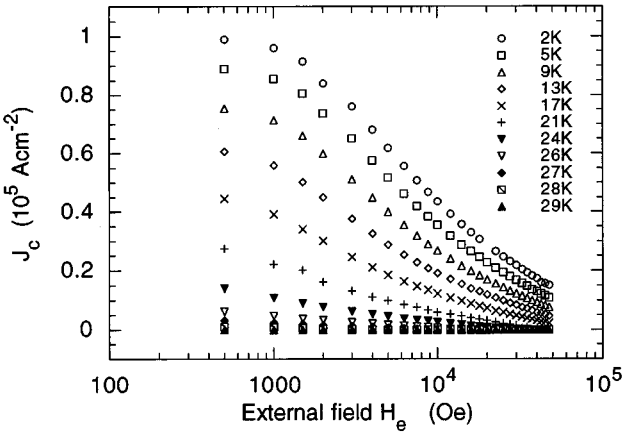

FIG. 8. Magnetic-field dependence of the hysteretically determined critical current density J_c at varied fixed temperature.

$M(H)$ curves at 5 K measured by Sparn *et al.*,[6] Politis, Sokolov, and Buntar[15] and this work in Fig. 7. We plot the normalized magnetization: $-M(H)/M(H_e=0.02T)$ as a function of the external applied field, H_e. A linear $M(H)$ is clearly observed for our crystal out to larger values of H_e. This clearly implies a higher H_{c1} for our crystal than for powder samples. If one includes effects of demagnetization, ${}_1D=0.57$ for our data and $D=1/3$ for the data of Refs. 6 and 15, an even more pronounced difference is observed. For reasons discussed below we believe that the single-crystal data offer a more reliable estimate of H_{c1} for a bulk sample of Rb_3C_{60}.

It is well known that, for small particles the lower critical field is a single-grain property, and depends on the grain size and geometry. A typical grain size of fullerene powder sample is $\sim 1\ \mu$m. Those samples may have compositional fluctuations and/or second phase, well below the detection limits of many characterization techniques yet still contribute to the pinning and/or ''dirty limit''.[22] For a dirty-limit sample the mean free path of electrons is comparable with or smaller than intrinsic coherence length. The effective penetration depth for a dirty-limit sample is larger by a factor $(1+\xi/l)^{1/2}$ (where l is the mean free path of electrons) than would be obtained by a ''clean-limit'' sample.[12] Assuming the minimum possible value of mean free path $l\approx 101$ Å (the C_{60} separation in the fcc lattice) and the experimental coherence length $\xi_{\mathrm{GL}}=27.7$ Å, this factor is about 2. This value is very close to the deviation of values of penetration depth obtained in single-crystal sample and the powder samples.[6] We observe that our millimeter-sized single crystal has a larger H_{c1} corresponding to a smaller effective penetration depth, which indicates experimental values are better described using the clean-limit analysis. Granular effects strongly influence the magnetic properties of samples in the intermediate-field regime and therefore the analysis of their critical field behaviors as well. We will discuss this topic more fully in the future.

D. Pinning and magnetic relaxation

We show typical hysteresis curves for our single-crystal sample in Fig. 3. The shape of the hysteresis curve indicates a quickly decreasing critical current density J_c of this single crystal with increasing field. A roughly exponential decrease in $J_c(H_e)$ is observed. This steep field dependence has been almost universally observed in weakly pinned HTSC materials.[9] It is indicative of a shielding current which has relaxed significantly from its critical value during the duration of the magnetization experiment. We therefore expect and do observe large magnetic relaxation rates for this crystal. While the current density derived from hysteresis measurements is certainly not critical, the geometric arguments of the Bean or critical-state models should be appropriate. For a slab geometry (of width a and length b) sample the critical current density in the ab plane can be calculated by an extended Bean model[9]

$$J_c=\frac{20\Delta M}{a(1-a/3b)},\quad a<b. \tag{8}$$

Here a and b are the width and length (in cm) of the superconductor, respectively, $\Delta M=M_+-M_-$ is the width of the hysteresis loop in emu/cm^3 (G) and J_c is reported in units of A/cm^2. M_+ and M_- are the hysteretic magnetization at an external field H_e. We show the magnetic-field dependence of critical current at varied fixed temperatures in Fig. 8. An evaluated value of ${}_1J_c(H=0)=1\times 10^5$ A cm^{-2} at $T=5\,K$ is an order of magnitude smaller than that of a powder sample reported by Sparn.[6] This is attributed to the fast relaxation in our pristine crystal. It is consistent with the notion that powder samples in the dirty limit may have many more flux-pinning sites than pristine single crystals. It is emphasized that our data reflects a bulk property of the sample instead of that of a collection of small particles. These pristine crystals therefore may be ideal candidates for studies in which pinning sites are artificially introduced, i.e., through irradiation-induced damage.[23,24]

A lower density of the effect pinning center in our single crystal might be responsible for decreasing ${}_1J_c$. The weak flux pinning in the Rb_3C_{60} single crystal is also evident in measurements of magnetic relaxation in various fixed fields

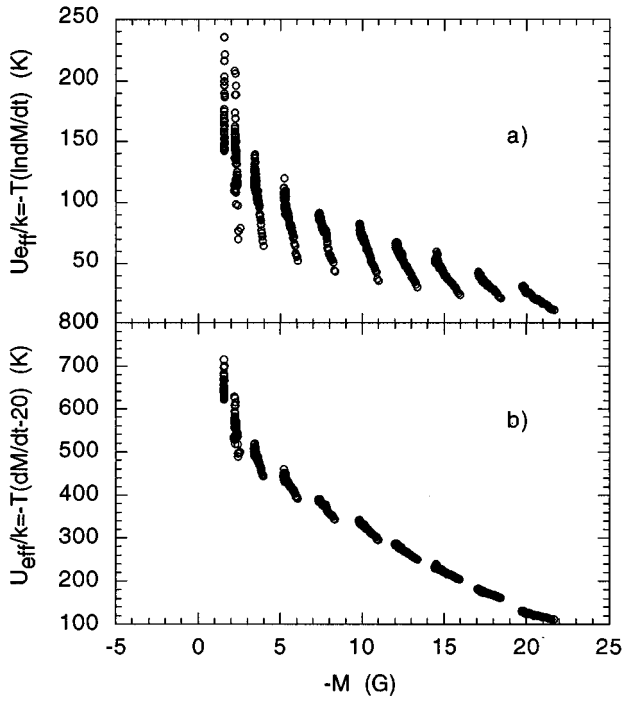

FIG. 9. (a) Estimate of ${}_1U_{\rm eff}(J)$ as determined from measurements of the time-dependent magnetic relaxation ${}_1M(t,T)$, using expression (10), for a fixed field of 4.0 T. (b) A constant $c=\ln(H\nu_0 a/2\pi a)=20$ is used to fit the data in (a).

and temperatures. In general, the rate of change of average flux density (induction, $\langle B\rangle$) in the superconductor with a slab geometry (of width a) is governed by a nonlinear magnetic-flux diffusion equation.[9,10] This can be derived considering a thermally activated (Arrhenius law) for the fluxon velocity and integration of the divergence theorem relationship for flux conservation finally yielding

$$\frac{d\langle B\rangle}{dt}=4\pi\frac{dM}{dt}=\frac{2Ha_0\nu_0}{a}\exp\left[\frac{U_{\rm eff}(j_s,H)}{kT}\right]. \qquad (9)$$

Here a_0 is a characteristic fluxon hop distance, ν_0 is a hopping attempt frequency, and $H=H_e$ is the external field boundary condition. Following Refs. 9 and rearranging Eq. (9) yields

$$\frac{U_{\rm eff}}{k}=-T\left[\ln\left|\frac{dM(t)}{dt}\right|-\left(\frac{H\nu_0 a_0}{2\pi a}\right)\right], \qquad (10)$$

which is used as the algorithm for obtaining the effective-pinning potential $U_{\rm eff}$, from $M(t)$ data recognizing that the argument of the second logarithm is slowly varying for fixed field and $T\ll T_c$. $U_{\rm eff}(J,H)$ is an effective-pinning potential which depends explicitly on current density J and external field H and implicitly on temperature. Here we take the constant $c=\ln(H\nu_0 a_0/2\pi a)$ as a temperature-independent scale constant in a first attempt at fitting this data. This has been shown to be a very rough approximation. As an example, the J-dependent $U_{\rm eff}$ from magnetic relaxation data of our sample is shown in Fig. 9. This data (as of yet uncorrected with an appropriate temperature scaling) still does indicate that $U_{\rm eff}(J,H)$ is a strongly nonlinear function as is the case for other high-temperature oxide superconductors. We will discuss a more elaborate scaling of $U_{\rm eff}$ with field and temperature in the future.

IV. SUMMARY

A comparison of the thermodynamic superconducting parameters for our crystal and powder samples reported in the literature is given in Table I. Here the thermodynamic critical field H_c is defined as $H_c{}^2=H_{c1}H_{c2}/\ln\kappa$. We conclude that the Rb_3C_{60} materials are all extremely type-II superconductors. Uncertainty in these length scales is likely due to variable sample quality (i.e., doping inhomogeneity) and granular effects. In conclusion, we have prepared and characterized high-quality single crystal Rb_3C_{60} with a size near 1 mm. We believe the thermodynamic superconducting parameters for Rb_3C_{60} extracted from our single-crystal data are more reflective of the intrinsic material properties.

We note that, field orientation effects and the three-dimensional character of Rb_3C_{60} superconductivity have been measured. The thermodynamic critical field H_c for the superconducting phase should be independent of field orientation. The slight difference between ${}_1H_c$ and ${}_2H_c$ in our data can be potentially explained by some differences in the distribution and orientation of defects in our crystal. Possible crystalline anisotropy effects on the vortex lattice structure (which depends on the applied field) and the morphology of

TABLE I. Superconducting state parameters of Rb_3C_{60}.

Parameter	Value, Field orientation [111]	Value, Field orientation [11$\bar{2}$]	References, random
T_c (K)	30.0	30.0	29.6 (Ref. 6), 28.4 (Ref. 20), 28 (Refs. 15 and 21)
H_{c1} (T)	0.050	0.047	0.012 (Ref. 6), 0.016 (Ref. 21), 0.045 (Ref. 15)
H_{c2} (T)	43	39	78 (Ref. 6), 55[a] (Ref. 20), 76 (Ref. 20), 44 (Ref. 15), 46.5 (Ref. 21), 38[a] (Ref. 18), 42 (Ref. 18)
H_c (T)	0.76	0.71	0.44 (Ref. 6), 0.41 (Ref. 21)
dH_{c2}/dT (T)/K	−2.08	−1.90	−3.9 (Ref. 6), 2.5 (Ref. 15)
$\xi_{(0)}$ (nm)	2.8	2.9	2.0 (Ref. 6), 2.3 (Ref. 15), 3.0 (Ref. 18)
$\lambda_{(0)}$ (nm)	109	113	247 (Ref. 6), 120–140 (Ref. 15)
$\kappa=\lambda_{(0)}/\xi_{(0)}$	39.2	39.1	124 (Ref. 6), 80.5 (Ref. 21)

[a]Exception to WHH upper critical field model.

our sample have not been considered in this work. Anisotropy effects on other magnetic properties of the fcc fullerene superconductors remain an open question to be explored. Comparison of the thermodynamic critical field, critical field, and Ginzburg-Landau parameters in different field orientations will be discussed more fully in subsequent work.

ACKNOWLEDGMENTS

The authors would like to thank M. A. Forman for his help with the pure C_{60} crystal growth. M.E.M. would like to thank the National Science Foundation for support of this work through NYI Award No. DMR-9258450.

[1] A. F. Hebard, M. J. Rosseinsky, R. C. Haddon, D. M. Murphy, S. H. Glarum, T. T. M. Palstra, A. P. Ramirez, and A. R. Kortan, Nature (London) **350**, 600 (1991).

[2] K. Hobard, O. Klein, S. M. Huang, R. B. Kaner, K. J. Fu, R. L. Whetter, and F. Diederich, Science **252**, 1154 (1991).

[3] M. J. Rosseinsky, A. P. Ramirez, S. H. Glarum, D. W. Murphy, R. C. Haddon, A. F. Hebbard, T. T. M. Palstra, A. R. Kortan, S. M. Zahurak, and A. V. Makhija, Phys. Rev. Lett. **66**, 2830 (1991).

[4] Katsumi Tanigaki, Mater. Sci. Eng. B **19**, 135 (1993).

[5] K. Holczer, O. Klein, and G. Grüner, Phys. Rev. Lett. **67**, 271 (1991).

[6] G. Sparn, J. D. Thompson, R. L. Whetten, S,-M. Huang, R. B. Kaner, F. Diederich, G. Gruner, and K. Holczer, Phys. Rev. Lett. **68**, 1228 (1992).

[7] T. T. M. Palstra, R. C. Haddon, A. F. Hebard, and J. Zaanen, Phys. Rev. Lett. **68**, 1054 (1992).

[8] J. G. Hou, Vincent, H. Crespi, X,-D. Xiang, W. A. Vareka, G. Briceno, A. Zettl, and Marvin L. Cohen, Solid State Commun. **86**, 643 (1993).

[9] M. E. McHenry and R. A. Sutton, Prog. Mater. Sci. **38**, 159 (1994).

[10] M. P. Maley, J. O. Willis, H. Lessure, and M. E. McHenry, Phys. Rev. B **42**, 2639 (1990).

[11] M. E. McHenry, S. Simizu, H. Lessure, M. P. Maley, J. Y. Coulter, I. Tanaka, and H. Kojima, Phys. Rev. B **44**, 7614 (1991).

[12] M. Tinkham, *Introduction to Superconductivity* (McGraw-Hill, New York, 1975).

[13] C. J. van der Beek, M. P. Maley, M. E. McHenry, D. A. Huse, M. J. V. Menken, and A. A. Menovsky, Phys. Rev. Lett. **67**, 2383 (1991).

[14] U. Welp, W. K. Kwok, G. W. Crabtree, K. G. Vandervoort, and J. Z. Liu, Phys. Rev. Lett. **62**, 1908 (1989).

[15] C. Politis, A. I. Sokolov, and V. Buntar, Mod. Phys. Lett. **6**, 351 (1992).

[16] Z. Hao, J. R. Clem, M. W. McElfresh, L. Civale, A. P. Malozemoff, and F. Holtzberg, Phys. Rev. B **43**, 2844 (1991).

[17] N. R. Werthamer, E. Helfand, and P. C. Hohenberg, Phys. Rev. **147**, 295 (1966).

[18] C. E. Johnson, H. W. Jiang, K. Holczer, R. B. Kaner, R. L. Whetten, and F. Diederich, Phys. Rev. **46**, 5880 (1992).

[19] S. C. Erwin and W. E. Pickett, Science **154**, 842 (1991).

[20] S. Foner, E. J. McNiff, Jr., D. Heiman, S. M. Huanf, and R. B. Kaner, Phys. Rev. B **46**, 14 936 (1992).

[21] V. Buntar, U. Eckern, and C. Politis, Mod. Phys. Lett. **6**, 1037 (1992).

[22] W. E. Pickett, in *Solid State Physics: Advances in Research and Applications*, edited by Henry Ehrenreich and Frans Spaepen (Academic, Boston, 1994), Vol. 48.

[23] J.-W. Lee, H. S. Lessure, D. E. Laughlin, M. E. McHenry, S. G. Sankar, J. O. Willis, J. R. Cost, and M. P. Maley, Appl. Phys. Lett. **57**, 2150 (1990).

[24] H. S. Lessure, S. Simizu, B. A. Baumert, S. G. Sankar, M. E. McHenry, M. P. Maley, J. R. Cost, and J. O. Willis, IEEE Trans. Mag. **27**, 1043 (1991).